Spin-current interaction with a monodomain magnetic body: A model study

J. Z. Sun
IBM T. J. Watson Research Center, P.O. Box 218, Yorktown Heights, New York 10598
(Received 3 February 2000)

I examined the consequence of a spin-current-induced angular momentum deposition in a monodomain Stoner-Wohlfarth magnetic body. The magnetic dynamics of the particle are modeled using the Landau-Lifshitz-Gilbert equation with a phenomenological damping coefficient α. Two magnetic potential landscapes are studied in detail: One uniaxial, the other uniaxial in combination with an easy-plane potential term that could be used to model a thin-film geometry with demagnetization. Quantitative predictions are obtained for comparison with experiments.

I. INTRODUCTION

Recently it has been shown, both theoretically[1–5] and experimentally[6–9] that a spin-polarized current, when passing through a small magnetic conductor, will deposit its spin-angular momentum into the magnetic system. It causes the magnetic moment to precess or even switch direction. The nature of this interaction between the spin current and the ferromagnetic moment brings about a new set of precession dynamics, the details of which remain unexplored. In this paper, a model system is presented of a monodomain ferromagnetic body with its dynamics determined by the Landau-Lifshitz-Gilbert (LLG) equation. The spin-current-induced magnetic precession dynamics are examined, and the results obtained compared to controlled thin-film experiments. This study also brings quantitative insights to the potential use of spin-current injection as a method for magnetic writing.

Centimeter-gram-seconds units are used for this work. Variables are grouped in simple forms where the only relevant unit is the energy product. Therefore results should be readily translatable to meter-kilogram-seconds or any other engineering units. For numerical simulation a set of dimensionless variables are introduced to simplify discussion and to elucidate the basic physics. Table I gives a summary of these reduced variables.

II. MODEL DEFINITION

The ferromagnet is represented by a Stoner-Wohlfarth monodomain magnetic body with magnetization **M**, situated at the origin, as shown in Fig. 1. For volume calculation only, the body is assumed to have a size of l_m along the $\mathbf{e}_x$ directions, and a in both $\mathbf{e}_y$ and $\mathbf{e}_z$ directions, thus with a volume of $a^2 l_m$. Assume the shape of the body is close to isotropic, and the energy landscape experienced by **M** is described by three terms (independent of its geometric parameters a and l_m): an applied field **H**, a uniaxial anisotropy energy U_K with easy axis along the $\mathbf{e}_z$ direction, and an easy-plane anisotropy U_p in the $\mathbf{e}_y-\mathbf{e}_z$ plane, with $\mathbf{e}_x$ being its normal direction. The magnetization **M** is assumed to be constant in magnitude, its motion represented by a unit direction vector $\mathbf{n}_m=\mathbf{M}/|\mathbf{M}|$, which at any instant of time, makes an angle θ with the $\mathbf{e}_z$ axis, while the plane of **M** and $\mathbf{e}_z$ makes an angle φ with $\mathbf{e}_x$. Coordinates (θ,φ) completely describe the motion of **M** in time. A spin-polarized current J enters the magnetic body in the $-\mathbf{e}_x$ direction, with spin-polarization factor η, and the spin direction in the $\mathbf{e}_y-\mathbf{e}_z$ plane, making an angle ϕ with $\mathbf{e}_z$ axis. The current exits in the same direction, but with its average spin direction aligned to that of **M**. The self-induced magnetic field of the current is ignored here—this is reasonable as long as the magnetic body is small with dimension a below about 1000 Å, where the spin-current effect is expected to become dominant over the current-induced magnetic field.

The potential energy for **M** is $U=U_K+U_p+U_H$, where $U_K=K\sin^2\theta$ is the uniaxial anisotropy, with $K=(1/2)MH_k$, where H_k is the Stoner-Wohlfarth switching field. The easy-plane anisotropy is written as $U_p=K_p(\sin^2\theta\cos^2\varphi\text{-}1)$. The magnetic field is applied in the easy plane of $\mathbf{e}_y-\mathbf{e}_z$, making an angle of ψ with the easy axis $\mathbf{e}_z$. Thus $U_H=-\mathbf{M}\cdot\mathbf{H}=-MH(\sin\theta\sin\varphi\sin\psi+\cos\theta\cos\psi)$. Define $h=H/(2K/M)$ and $h_p=K_p/K$,

$$U(\theta,\varphi)=K[\sin^2\theta+h_p\sin^2\theta\cos^2\varphi-2h(\sin\theta\sin\varphi\sin\psi+\cos\theta\cos\psi)]. \quad (1)$$

TABLE I. Summary for dimensionless units.

Dimensionless variable	Conversion relation	Normalization quantity
Magnetization	$m=M/M_s$	Saturation magetization M_s
Magnetic field	$h=H/H_k$	Uniaxial-anisotropy field H_k
Easy-plane anisotropy field	$h_p=K_p/K=4\pi M_s/H_k$	Uniaxial-anisotropy field H_k.
Effective spin current	$h_s=(\hbar/2e)\eta J/l_m M_s H_k$	Uniaxial-anisotropy energy $M_s H_k/2$
Natural time unit	$\tau=\Omega_k t/(1+\alpha^2)$	Ferromagnetic resonance frequency $\Omega_k=\gamma H_k$

 ©2000 The American Physical Society

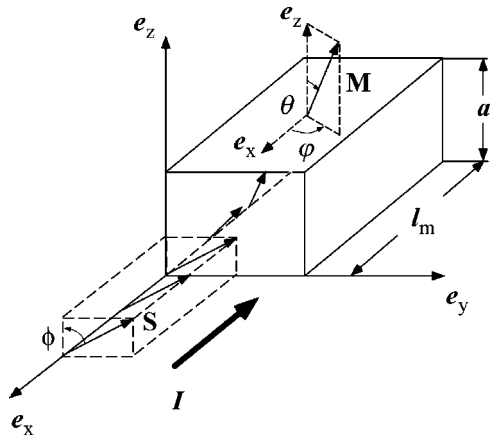

FIG. 1. Model geometry definition and related mathematical symbols.

If one takes the usual thin-film situation of shape anisotropy and lets the easy-plane anisotropy energy be $K_p=2\pi M_s^2$ then $h_p=4\pi M_s/H_k$. The torque $\mathbf{M}$ experiences within unit volume $l_m\times$(unit area) under potential well Eq. (1) can be written as

$$\frac{\mathbf{\Gamma}_U}{l_m}=-\mathbf{n}_m\times\nabla U(\theta,\varphi) \tag{2}$$

with $\nabla U(\theta,\varphi)=(\partial U/\partial\theta)\mathbf{e}_\theta+(1/\sin\theta)(\partial U/\partial\varphi)\mathbf{e}_\varphi$, where $\mathbf{e}_\theta$ and $\mathbf{e}_\varphi$ are unit vectors for θ and φ rotation, respectively.

The three terms in potential energy U lead to three terms in torque $\mathbf{\Gamma}_U$. First the uniaxial anisotropy term:

$$\frac{\mathbf{\Gamma}_1}{l_mK}=(2\sin\theta\cos\theta)[(\sin\varphi)\mathbf{e}_x-(\cos\varphi)\mathbf{e}_y]. \tag{3}$$

Second the easy-plane anisotropy term:

$$\frac{\mathbf{\Gamma}_2}{l_mK}=-2h_p[(\cos\theta\sin\theta\cos\varphi)\mathbf{e}_y-(\cos\varphi\sin\varphi\sin^2\theta)\mathbf{e}_z]. \tag{4}$$

Third, the applied field term:

$$\frac{\mathbf{\Gamma}_3}{l_mK}=2h[(\sin\varphi\cos\psi\sin\theta-\cos\theta\sin\psi)\mathbf{e}_x-(\cos\varphi\cos\psi\sin\theta)\mathbf{e}_y+(\sin\theta\cos\varphi\sin\psi)\mathbf{e}_z]. \tag{5}$$

Spin current also brings a torque to $\mathbf{M}$. We assume that the magnetic body absorbs the angular-momentum from the spin current *only in the direction perpendicular to* $\mathbf{M}$.[10] This causes a net torque on $\mathbf{M}$, which can be expressed in vector form as:

$$\mathbf{\Gamma}_4=s\mathbf{n}_m\times(\mathbf{n}_s\times\mathbf{n}_m)=2l_mKh_s\mathbf{n}_m\times(\mathbf{n}_s\times\mathbf{n}_m), \tag{6}$$

where $s=(\hbar/2e)\eta J$ is the spin-angular momentum deposition per unit time. $\eta=(J_\uparrow-J_\downarrow)/(J_\uparrow+J_\downarrow)$ is the spin-polarization factor of the incident current J. The spin direction of the incident current is in the $\mathbf{e}_y-\mathbf{e}_z$ plane, and makes an angle ϕ with the $\mathbf{e}_z$ axis. $\mathbf{n}_s$ is a unit vector whose direction is that of the initial spin direction of the current. Also we define

$$h_s=\frac{s}{2l_mK}=\frac{\left(\frac{\hbar}{2e}\right)\eta J}{2l_mK}=\frac{\left(\frac{\hbar}{2e}\right)\eta I}{2l_ma^2K} \tag{7}$$

as the spin-current amplitude in dimensionless units. In component form Eq. (6) becomes

$$\frac{\mathbf{\Gamma}_4}{l_mK}=2h_s\{-(\sin\theta\cos\varphi)(\sin\theta\sin\varphi\sin\phi+\cos\theta\cos\phi)\mathbf{e}_x+[(\cos\theta)(\sin\phi\cos\theta-\cos\phi\sin\theta\sin\varphi)+\sin^2\theta\cos^2\varphi\sin\phi]\mathbf{e}_y+[(\sin\theta)(\sin\theta\cos\phi-\sin\varphi\sin\phi\cos\theta)]\mathbf{e}_z\}. \tag{8}$$

The dynamics of $\mathbf{M}$ under the influence of torque

$$\mathbf{\Gamma}=\sum_{i=1}^{4}\mathbf{\Gamma}_i$$

can be described using the Landau-Lifshitz-Gilbert equation as

$$\frac{d\mathbf{n}_m}{dt}+\alpha\left(\mathbf{n}_m\times\frac{d\mathbf{n}_m}{dt}\right)=\frac{1}{2}\Omega_K\sum_{i=1}^{4}\left(\frac{\mathbf{\Gamma}_i}{l_mK}\right), \tag{9}$$

where α is the LLG damping coefficient and $\gamma=g\mu_B/\hbar$ is the gyromagnetic ratio. In our case, $g=2$. Here we introduced a characteristic frequency unit $\Omega_K=\gamma H_k$. Equation (9) can be written in component form using a natural time unit $\tau=\Omega_Kt/(1+\alpha^2)$:

$$\begin{bmatrix}\theta'\\ \varphi'\end{bmatrix}=\sum_{i=1}^{4}\begin{bmatrix}\theta_i'\\ \varphi_i'\end{bmatrix} \tag{10}$$

with

$$\begin{bmatrix}\theta_1'\\ \varphi_1'\end{bmatrix}=-\begin{bmatrix}\alpha\sin\theta\cos\theta\\ \cos\theta\end{bmatrix},$$

$$\begin{bmatrix}\theta_2'\\ \varphi_2'\end{bmatrix}=-h_p\begin{bmatrix}(\sin\varphi+\alpha\cos\theta\cos\varphi)\sin\theta\cos\varphi\\ (\cos\varphi\cos\theta-\alpha\sin\varphi)\cos\varphi\end{bmatrix},$$

$$\begin{bmatrix}\theta_3'\\ \varphi_3'\end{bmatrix}=-h\begin{bmatrix}\cos\varphi\sin\psi\\ +\alpha(\sin\theta\cos\psi-\cos\theta\sin\varphi\sin\psi)\\ [(\sin\theta\cos\psi-\cos\theta\sin\varphi\sin\psi)\\ -\alpha\cos\varphi\sin\psi]/\sin\theta\end{bmatrix},$$

$$\begin{bmatrix}\theta_4'\\ \varphi_4'\end{bmatrix}=h_s\begin{bmatrix}\alpha\cos\varphi\sin\phi\\ +\sin\varphi\sin\phi\cos\theta-\cos\phi\sin\theta\\ (\cos\varphi\sin\phi\\ -\alpha\sin\varphi\sin\phi\cos\theta)/\sin\theta\\ +\alpha\cos\phi\end{bmatrix},$$

where $()' = d/d\tau()$. Equation (10) can be numerically evaluated. It is the basis for all numerical studies discussed below.

III. ANALYTICAL RESULTS

In this section we discuss the analytical solutions to Eq. (10). For simplicity we only consider the on-axis geometry where both applied field $\mathbf{h}$ and the spin direction $\mathbf{n}_s$ are along the easy-axis $\mathbf{e}_z$. Further, we assume a small cone-angle limit $|\theta| \ll 1$. In this case Eq. (10) becomes

$$\frac{d\theta}{d\tau} = -\theta[\alpha(1+h) + h_p(\sin\varphi + \alpha\cos\varphi)\cos\varphi + h_s]$$
$$\frac{d\varphi}{d\tau} = -1 - h_p(\cos\varphi - \alpha\sin\varphi)\cos\varphi - h + h_s\alpha. \tag{11}$$

A coordinate transformation of $u_1 = \theta\cos\varphi$ and $u_2 = \theta\sin\varphi$ could further simplify this equation set for small cone-angle motion. However, we decide to keep using the polar coordinate system here, as it allows easy comparison with numerical results that involve large cone-angle motions.

A. Unperturbed equation of motion

In this case, $\psi = 0$, $h_s = 0$, and $\alpha = 0$. For finite h_p, Eq. (11) can be solved to give

$$\varphi(\tau) = \arctan\left[\left(\frac{\varepsilon+1}{\varepsilon}\right)^{1/2}\cot\ \omega_p\tau\right]$$
$$\theta(\tau) = \theta_0\left[\frac{(2\varepsilon+1)+\cos 2\omega_p\tau}{2(\varepsilon+1)}\right]^{1/2} \tag{12}$$

and in implicit form simply from energy considerations:

$$\theta^2 = \frac{\varepsilon\theta_0^2}{(\varepsilon+\cos^2\varphi)}, \tag{13}$$

where $\varepsilon = (1+h)/h_p$ and $\omega_p = h_p\sqrt{\varepsilon(1+\varepsilon)}$. An initial condition of $\theta = \theta_0 \ll 1$ and $\varphi = \pi/2$ is assumed.

This derivation is valid only for $\varepsilon > 0$, that is for $h > -1$. Similar small θ orbits can be obtained for $\varepsilon \ll -1$ with $\varepsilon(1+\varepsilon) > 0$. We will restrict our discussion to these two regions. When $\varepsilon(1+\varepsilon) < 0$, the trajectory changes shape to include large oscillations in θ, violating the small θ assumption. This corresponds to an unperturbed orbit crossing the equator with periodic oscillations of $\mathbf{M}$ from $\mathbf{e}_z$ to $-\mathbf{e}_z$ direction.

B. Average system energy

Use the constant-energy motion trajectory [Eqs. (12) and (13)] as a starting point, and treating the damping and spin current as a perturbation, the average rate of energy change $\langle dU/d\tau\rangle$ is obtained using Eq. (1), with Eq. (11) for θ' and φ'. The average energy variation rate thus obtained is

$$\frac{1}{K}\left\langle\frac{dU}{d\tau}\right\rangle = -(2h_p\varepsilon\theta_0^2)h_s - (2h_p\varepsilon\theta_0^2)\alpha h_p\left[-\varepsilon(1+\varepsilon)A + (1+2\varepsilon) + \frac{h_s}{h_p^2}B\right] \tag{14}$$

with

$$A \equiv \left\langle\frac{1}{\varepsilon+\cos^2\varphi}\right\rangle = \frac{2\varepsilon+1}{2\varepsilon(1+\varepsilon)}$$
$$B \equiv \left\langle\frac{\cos\varphi\sin\varphi}{\varepsilon+\cos^2\varphi}\right\rangle = 0 \tag{15}$$

as long as $\varepsilon(\varepsilon+1) > 0$. Therefore,

$$\frac{1}{K}\left\langle\frac{dU}{d\tau}\right\rangle = -2(1+h)\left[\left(1+h+\frac{1}{2}h_p\right)\alpha + h_s\right]\theta_0^2. \tag{16}$$

C. Low-field switching threshold

For $|h| < 1$, Eq. (16) gives the on-axis stability threshold for spin-current-driven motion at the small cone-angle limit. For spin current, instability occurs when the magnitude of h_s exceeds a critical value. In this case,

$$h_s < h_{sc} = -(1+h+\tfrac{1}{2}h_p)\alpha. \tag{17}$$

Placing real-life units back in, we have for the magnitude of the critical spin-injection current:

$$I_c = \frac{1}{\eta}\left(\frac{2e}{\hbar}\right)\frac{\alpha}{|\cos\phi|}(a^2 l_m H_k M_s)\left(1+\frac{2\pi M_s}{H_k}+\frac{H}{H_k}\right), \tag{18}$$

which was the same as shown in Ref. 7 but now also includes an easy-plane anisotropy $2\pi M_s/H_k$. This relation is also consistent with the results obtained by Katine *et al.*[9]

It is curious to notice that the easy-plane anisotropy h_p does not affect the magnetic switching threshold of $|h| = 1$, yet it does affect the threshold for spin-current-induced switch. For large easy-plane anisotropy $|h_{sc}| \approx \alpha h_p/2$. This is because a magnetic-field-driven switch can occur with $\mathbf{M}$ practically rotating only in the easy plane, whereas a spin-current-induced switch has to involve significant amount of out-of-plane precession.

It is also important to mention that Eq. (17) only gives a threshold for an instability towards an increasing cone angle in small θ limit. It does not guarantee that the cone angle will increase indefinitely and a switching event will follow. For large h_p systems the actual switching requires a spin current with larger magnitude than dictated by Eq. (17), as will be discussed later using a numerical example.

D. High-field switching threshold

For $|h| \gg h_p + 1$, and with a large spin-current h_s pushing the moment in the opposite direction as h does, one obtains another threshold, either for current or for applied field, for the high-field forced alignment of $\mathbf{M}$ with respect to applied field. This relates to the stable small cone-angle ($\theta_0 \ll 1$) solution for the unperturbed ($\alpha = 0$, $h_s = 0$) orbit in the limit

of $\varepsilon(\varepsilon+1)>0$ but $\varepsilon<-1$. In this case, because **M** and h are in opposite directions along the easy axis, a small θ_0 stability corresponds to an energy *maximum*. Using Eq. (16) and keeping track of the signs with regard to the relative alignment of **M** and h, one gets the threshold fields for field-induced switching under a large spin current h_s:

$$|h_{ac}^{(\pm)}| = \frac{|h_s|}{\alpha} \pm \left(1+\frac{1}{2}h_p\right), \tag{19}$$

where $h_{ac}^{(+)}$ is the threshold field for **M** to switch from antiparallel to parallel to an h increasing in magnitude, while $h_{ac}^{(-)}$ is the threshold field for switching of M back from a parallel to antiparallel state with respect to h as the value of h is reduced. In real-life units, if one assumes a zero-field threshold current $I_c \propto 2\pi M_s$, then Eq. (19) can be rewritten as

$$H_{ac}^{(\pm)} = 2\pi M_s\left(\frac{I_{bias}}{I_c} \pm 1\right), \tag{20}$$

where I_{bias} is the bias current of the junction. Equations (19) and (20) are related to the intermediate magnetoresistance states observed in Fig. 3(d) of Ref. 9, as will be discussed below using a numerical example.

IV. NUMERICAL STUDIES

Numerical studies of Eq. (10) are organized as follows. First we discuss the time evolution of the magnetization **M**. This is followed by a study on the effect of spin current on the magnetic switching, both in terms of sweeping field **H** and sweeping current h_s. We then discuss the speed of switching under spin-current drive as it compares to the more familiar field-driven reversal process. In the end we briefly discuss the device and material implications of this mechanism.

We use the reduced units introduced in previous sections for our simulation. A summary of the units and their reference values are given in Table I. In most simulation results discussed below we set the LLG damping coefficient $\alpha = 0.01$, unless differently specified for individual cases.

A. Time evolution of M under the influence of a spin-current

First consider the simple uniaxial anisotropy case with $h_p=0$. The time evolution of **M** under the influence of a uniaxial anisotropy field is one of a spiral motion traced by the tip of **M**. The damping action causes a decrease of the cone angle, and the moment eventually comes to rest in the direction parallel to the easy-axis $\mathbf{e}_z$. This is well known. Under the influence of a spin-current h_s, **M** will pick up an additional precession corresponding to the spin-angular momentum deposition. The balance between the damping term and that of h_s determines the final resting direction of **M**, as described by

$$\frac{d\theta}{d\tau} = -\theta[\alpha(1+h)+h_s]$$
$$\frac{d\varphi}{d\tau} = -(1+h)+h_s\alpha \tag{21}$$

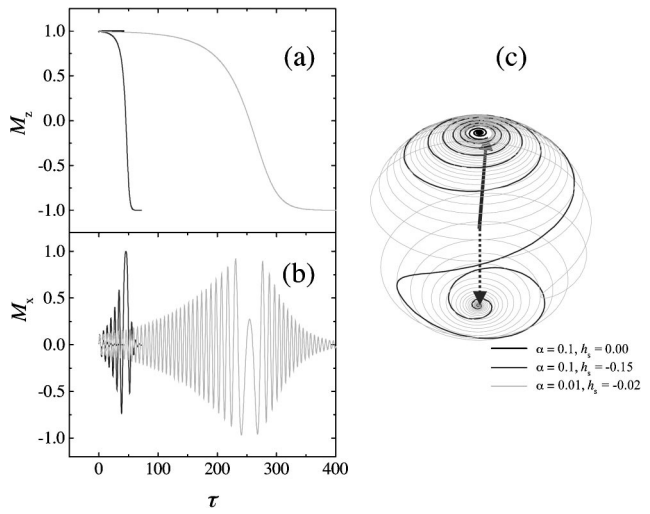

FIG. 2. The precession of magnetization under the influence of a spin current. Uniaxial anisotropy alone. (a) Time dependence of M_z. (b) Time dependence of M_x. (c) A 3D portrait of the spiral motion of the tip of **M**. North pole is $\mathbf{e}_z$ direction.

that has a solution of

$$\theta(\tau) = \theta_0 \exp(-\tau/\tau_1)$$
$$\tau_1 = 1/[\alpha(1+h)+h_s] \tag{22}$$

with a threshold spin current of

$$h_{sc} = -\alpha(1+h). \tag{23}$$

Given an initial state such that **M** is stationary and slightly tilted away from the uniaxial direction $\mathbf{e}_z$ at $\tau=0$, the time-dependent evolution of $\mathbf{M}(\tau)$ is illustrated in Fig. 2 for different values of spin current h_s. A characteristic of a spin-current-induced switch of $\mathbf{M}(\tau)$ is the reversal of its precession direction when it crosses the equatorial position. This comes from the sign change in the spin-current-induced torque term in Eq. (6). A purely magnetic-field-driven switch of $\mathbf{M}(\tau)$ does not have this precession reversal.

For finite values of h_p, as one may expect, the precession in general follows an elliptically distorted trajectory, with the cone angle more spread out in the easy plane, while becoming confined normal to the easy plane. An example of this situation is shown in Fig. 3. Later we will show that a large $h_p(\gg 1)$ does not only compress the precession cone angle into the easy plane, it can also introduces a steady-state precession for spin currents with a magnitude slightly above the low-cone-angle stability threshold h_{sc} from Eq. (17).

B. Spin-current induced switching

As shown above, in the case of pure uniaxial anisotropy with the spin polarization aligned to that of the easy axis, when h_s exceeds h_{sc}, **M** switches its orientation to become aligned with the spin-polarization. This can be traced out as an hysteresis loop in $\mathbf{M}(h_s)$, as shown in Fig. 4. A systematic dependence of the switching field h_{sc} on applied field h is found, following Eq. (23).

For $h=0$, $\mathbf{M}(h_s)$ is always symmetric against origin. That does not necessarily mean $\mathbf{M}(I)$ is symmetric. This is because the amount of net torque deposition depends sensi-

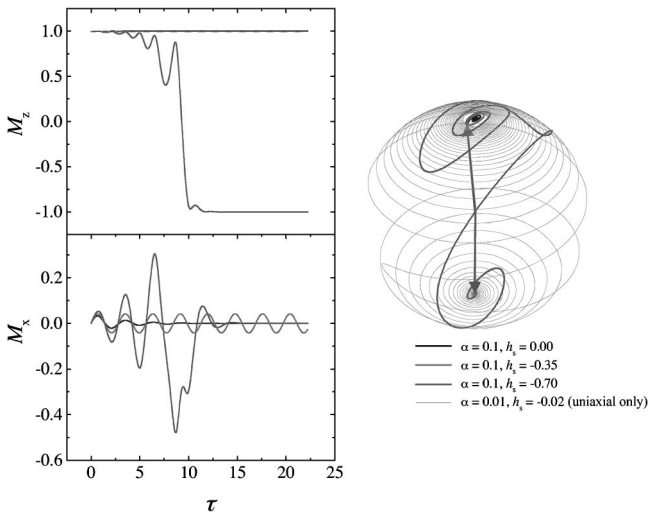

FIG. 3. The precession of magnetization under the influence of a spin current. Uniaxial anisotropy plus an easy-plane anisotropy of $h_p=5$. The uniaxial-anisotropy-alone trace of $\alpha=0.01$ is included for comparison. The elliptical precession is apparent here, with the cone-angle being compressed in the direction normal to the easy plane. Panels have the same definition as in Fig. 2.

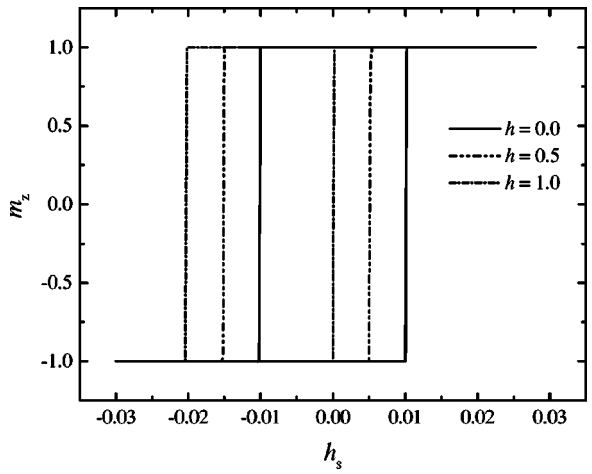

FIG. 4. Spin-current-driven reversal of magnetization. Uniaxial anisotropy only, no easy-plane anisotropy is added. The switching current h_{sc} shows linear dependence on applied easy-axis field h as predicted by Eq. (23).

tively on the condition of the interface responsible for spin-current injection. This situation can be phenomenologically handled by introducing an effective spin polarization containing a sign dependence on I, i.e., $\eta\rightarrow\eta_{\pm}$ in Eqs. (7) and (18).

C. The effect of a strong easy-plane anisotropy

The hysteresis loop $\mathbf{M}(h_s)$ changes its shape upon the introduction of a large easy-plane anisotropy. This is illustrated in Fig. 5. For $h_p>5$, before a complete reversal of $\mathbf{M}$, a sloped $\mathbf{M}(h_s)$ region is seen to develop when $|h_s|$ first exceeds $|h_{sc}|$ as defined by Eq. (17). This region corresponds to a steady-state precession with an oblong-shaped trajectory. This can be seen in the time dependence of $M_z(\tau)$, as shown in Fig. 6.

This large angle steady-state precession is a result of an increase in effective damping for large cone-angle dynamics. As one increases the easy-plane anisotropy, the precession becomes increasingly nonlinear and complex, which channels more energy into the higher frequency modes that give more dissipation to $\mathbf{M}(\tau)$ per unit time. A balance can always be established between increased energy injection from increasing h_s and the increased damping from increasing cone angle, as long as the maximum cone angle does not cross the equator. This is the region where a steady-state precession is formed. Once the precession crosses the equator, however, due to the sign change of the torque term [Eq. (6)], the precession accelerates, and a switching of $\mathbf{M}(\tau)$ results.

Figure 5 also shows the dependence of $\mathbf{M}(h_s)$ hysteresis on applied field h. While Eq. (17) does dictate the onset of $\mathbf{M}$ reversal (see bottom inset, Fig. 5), the threshold current position corresponding to the completion of $\mathbf{M}$ reversal (defined as $h_{sc1,2}$ shown in Fig. 5) does not follow from that of Eq. (17), but rather has a stronger dependence in h, as shown in Fig. 5. Furthermore, the dependence of $h_{sc1,2}$ on applied field h is asymmetric. When the direction of h is to decrease h_{sc2}, the magnitude of h_{sc} decreases asymptotically towards $h_{sc}=-\alpha(1+h+\frac{1}{2}h_p)$ from Eq. (17). It does not decrease below h_{sc} however until $h<-1$. Then a sudden switch occurs and h_{sc2} drops to zero. This is reasonable, since $h<-1$ is the condition for a magnetic-field induced moment reversal without the assistance of spin current, naturally h_{sc2} becomes zero. On the other hand, if h is to increase the magnitude of h_{sc1}, as occurred on the left-side transition shown in Fig. 5, h_{sc1}'s change is not bounded by h_{sc}, hence larger field dependence in the (broadened) switching field is observed there.

D. High-field switching threshold

An example of the simulated high-field switching threshold behavior is shown in Fig. 7. Here a large spin current $h_s=6.0$ is applied with its polarization along the $-\mathbf{e}_z$ direction. Also included is an easy-plane anisotropy of $h_p=190$. The applied field is swept from -800 to 800 along the $\mathbf{e}_z$ axis. This is a situation very similar in quantitative terms to the experiment shown in Fig. 3(d) of Katine *et al.*'s paper.[9] The $\mathbf{M}(h)$ behavior consists of four regions.

(1) For $h<0$ in Fig. 7, the effect of both applied field and the spin current is to force $\mathbf{M}$ to point to -1, hence $\mathbf{M}$ points to $-\mathbf{e}_z$.

(2) Between $h=0$ and $h=h_p$: This region corresponds to an unperturbed orbit involving large cone angles where $\varepsilon<0$ and $\varepsilon(1+\varepsilon)<0$. In the present situation, the competition between applied field h which now favors a $+1$ direction for $\mathbf{M}$, and that of the spin current (still pointing towards $-\mathbf{e}_z$) causes a strong steady-state precession when $1<h\ll h_p$. As $h\rightarrow h_p$ a stable resting position develops for $\mathbf{M}$ that points out of the easy plane and making an angle with the $-\mathbf{e}_z$ direction, results in an M_z value between 0 and -1. As h increases in value, $\mathbf{M}$ increasingly tilts back towards $-\mathbf{e}_z$, away from h, causing M_z to approach -1. It is at first counterintuitive that M_z in this region should become closer to -1 as the applied field is being increased. But this is actually not surprising once one realizes that in this region

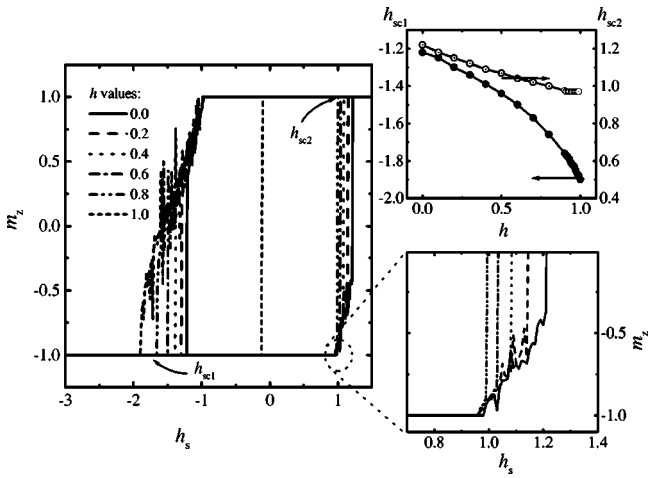

FIG. 5. Spin-current induced magnetic switching hysteresis loop $\mathbf{M}(h_s)$, with a strong easy-plane anisotropy $h_p=190$ (chosen to emulate a cobalt thin-film's demagnetization field $4\pi M_s$). The onset position in h_s for $\mathbf{M}$ switching follows the estimate given in Eq. (17). It is not very sensitive to the change of h from 0 to 1, as expected (since $h \ll h_p$ in this range of h). However, the beginning portion of the switching curve is much more gently sloped. This is due to the presence of a steady-state precession as discussed in the text and in Fig. 6.

the behavior of $\mathbf{M}$ under the influence of h_s is to seek a resting position with energy *maximum*.

(3) Between $h=h_p$ and $h=h_{ac}^{(+)}=|h_s|/\alpha+(1+h_p/2)$, following Eq. (19). In this region M_z is completely forced to -1.

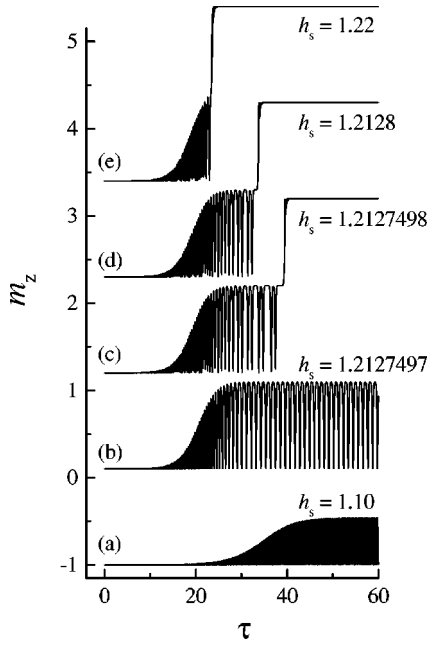

FIG. 6. The evolution of steady-state precession and the completion of $\mathbf{M}(h_s)$ switch as the precessing moment crosses equator upon increasing h_s. Initial $\theta=\pi-0.01$. Small deviation from π is added to shorten the initial build-up time for precession amplitudes. Curves (b)–(e) are progressively offset in vertical direction. A crossover from steady-state precession and complete switching occurs within $1.2127497<h_s<1.212\,7498$.

(4) When $h>h_{ac}^{(+)}$, where finally the effect of applied field takes over, and $\mathbf{M}$ switches direction to rest along the direction of applied field, and $M_z=+1$.

Once $\mathbf{M}$ switches direction to align with h, the stability criteria for small cone angle, Eq. (16) changes sign, hence on its way back, $h_{ac}^{(-)}=|h_s|/\alpha-(1+h_p/2)$.

The monodomain threshold $h_{ac}^{(\pm)}$ can only give a rough estimate to the high-field threshold observed in Katine *et al.*'s experiment. For a real thin-film sample such as the one used by Katine *et al.*, the magnetic dynamics between $h=0$ and $h=h_{ac}^{(\pm)}$ is not even approximately monodomain in nature. This is because in this region large cone-angle motion as well as resting positions with significant out-of-the-plane component of $\mathbf{M}$ is involved, which would favor spin-wave excitation or domain formation. The fact that the system in this parameter region seeks out an energy maximum rather than a minimum, further increases the likelihood for the film to break into complex domains or to excite spin waves. This may account for the wide plateau observed in Ref. 9. A proper treatment of these is however beyond the scope of this paper.

E. Effect of spin current on the M(H) switching characteristics: Spin-current-induced distortion to astroids

Here we study the switching behavior of $\mathbf{M}(\mathbf{H})$ as a function of spin current h_s. We focus on on-axis geometries, where the relative angle ϕ between $\mathbf{n}_s$ and $\mathbf{e}_z$ is either zero or π.

Without the presence of a spin current, the $\mathbf{M}(\mathbf{H})$ switching characteristic for simultaneous easy- and hard-axis field presence is an analytically solvable energy minimum problem.[11] The resulting switching boundary forms an astroid shape, with the boundary curves defined by

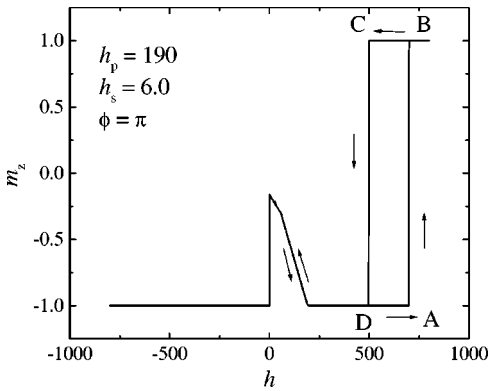

FIG. 7. Numerical result for the high-current, high-field behavior. Field h is applied along $\mathbf{e}_z$. Spin-current polarization is along $-\mathbf{e}_z$. From origin to $h=h_p$, the competition between applied field and the spin-current causes a deflected final resting angle for the moment. Between $h=h_p$ and point A with $h_A=h_{ac}^{+}=(h_s/\alpha)+(1+h_p/2)$ according to Eq. (19), spin-current effect causes the moment to seek out the energy maximum for its resting direction, hence $m_z=-1$. At point A, the energy term from applied field finally takes over, and a switching of magnetic moment from -1 to 1 occurs. This switching is hysteretic—upon reversing the sweep direction of applied field, the moment does not switch back to -1 until point C where $h_C=h_{ac}^{-}=(h_s/\alpha)-(1+\frac{1}{2}h_p)$. The net hysteresis opening between points A and C is $\delta h=h_p+2\sim h_p$.

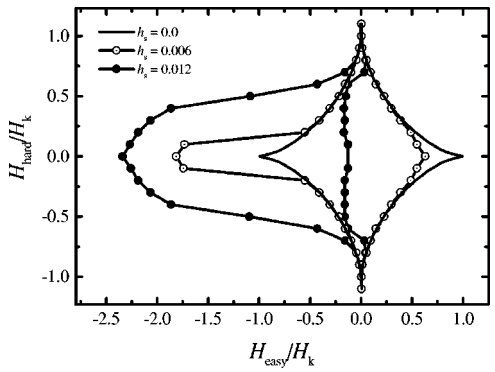

FIG. 8. Uniaxial anisotropy only: effect of spin-current injection on the shape of **M**(**H**). The zero-current switching characteristics reproduces the well-known ''astroid'' shape. For this simulation $\alpha=0.01$, thus $h_{sc}=0.01$.

$$h_{easy}^{2/3}+h_{hard}^{2/3}=1. \tag{24}$$

The effect of a spin current on the shape of the astroid is shown in Fig. 8, for a monodomain magnetic moment with only a uniaxial anisotropy term. Notice that the amount of spin current required to significantly change the shape of the astroid is within a factor of 2 of the zero-field critical current h_{sc}. The increase in magnitude of the switching field on the left side of the astroid is interesting to observe, as this is a region where the spin-momentum deposition completely changed the magnetic system's trajectory of motion, distorting significantly the astroid boundary. While without the presence of the spin current a large cone-angle precession will develop, the spin current stabilizes the small cone-angle precession, and hence this region is now treatable as a perturbation to the constant-energy trajectory.

The introduction of an easy-plane anisotropy h_p does not affect the zero-spin-current switching astroid [Eq. (24)]. However, it does alter the effect the spin current has on the shape of the astroid. The evolution of the switching characteristics for $h_p=190$ is shown in Fig. 9. The amount of spin current required to affect the shape of the astroid again is around the zero-field critical current h_{sc}, as determined by Eq. (17). The presence of a strong easy-plane anisotropy completely suppresses the increase of switching field magnitude on the left side of the astroid.

V. SWITCHING SPEED

The reversal of **M** under a spin-current-driven situation is different from that of a magnetic-field-driven case.

For field-driven reversal, in small damping limit ($\alpha\ll 1$), the reversal time for magnetization **M** along its easy axis depends primarily on the initial dynamics of the moment. For a system with $\varepsilon=(1+h)/h_p\lesssim 0$, the unperturbed orbit for small θ can be used to estimate the amount of time for the cone angle to evolve from its initial value θ_0 to θ. In the limit of $h_p\gg 1$, to the leading order of ε, it is

$$\tau(\theta)=\frac{1}{h_p\sqrt{-\varepsilon}}\ln\frac{\theta+\sqrt{\theta^2-\theta_0^2}}{\theta_0}. \tag{25}$$

Therefore the asymptotic behavior of the initial reversal-related switching time is (setting $\theta\sim 1$):

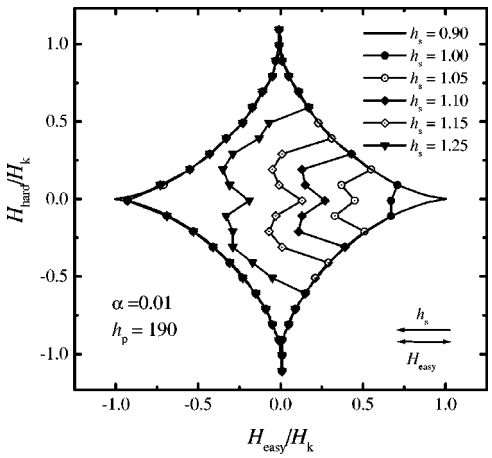

FIG. 9. Uniaxial anisotropy plus a strong in-plane anisotropy of $h_p=190$. The effect of spin-current injection on the shape of **M**(**H**) is quite different from those shown in Fig. 8 with only uniaxial anisotropy. In this case, $h_{sc}=0.96$ as calculated from Eq. (17).

$$\tau_0\approx\frac{1}{h_p\sqrt{-\varepsilon}}\ln\frac{1+\sqrt{1-\theta_0^2}}{\theta_0}\propto\begin{cases}|1-h|^{-1/2} & (h\to 1^+)\\ -\ln\theta_0 & (\theta_0\to 0^+).\end{cases} \tag{26}$$

This relation is verified by numerical simulation for a specific set of conditions: $h_p=190$ and $\alpha=0.01$ and 0.001, respectively, as shown in Fig. 10.

For current-driven reversal the process is somewhat different. Since current-driven reversal is determined by the balance of damping-related dissipation and the spin-current induced energy gain, damping plays a much more critical role—it determines the value of threshold h_{sc}. For the uniaxial anisotropy-only situation, Eq. (22) gives

$$\tau(\theta)\approx|h_s-h_{sc}|^{-1}\ln(\theta/\theta_0). \tag{27}$$

A similar scaling behavior is found numerically in the large h_p limit, as shown in Fig. 11.

To compare the situation between a field-driven reversal and a spin-driven switch, one examines the behavior of $\tau(\theta)$ for the same amount of relative overdrive amplitude in field and in spin current. Following Eq. (17), for a given amount of overdrive amplitude $|h_s|=(1+\delta)|h_{sc}|$, $\tau\propto(\alpha\delta h_p)^{-1}\ln(\theta/\theta_0)$, whereas for the same amount of overdrive in field $|h|=1+\delta$, $\tau\propto(\delta h_p)^{-1/2}\ln(2\theta/\theta_0)$. Thus for a spin-current switch with a fixed percentage of overdrive, the speed is directly proportional to its threshold current αh_p, and hence to α, whereas for magnetic-field-driven switch, α doesn't matter as long as $\alpha\ll 1$.

Another limit for a spin-current switch is when the current is well-above the threshold. In this case, $\tau_0\propto|h_s|^{-1}\ln(\theta/\theta_0)$. Thus in a large current limit, the switching time for a spin-injection process is independent of α, and is determined by the amount of spin current injected. Thus, in a large spin-current limit, the total amount of spins needed for a reversal event is independent of the magnitude of the spin current.

To get some feelings for real materials, consider a patterned cobalt film. Assume a uniaxial anisotropy field of $H_k=100$ Oe from the film's in-plane shape. In the direction perpendicular to the film, a demagnetization field of $4\pi M_s\approx 1.8\times 10^4$ Oe$\approx 180H_k$ is present, thus $h_p\approx 180$, similar to

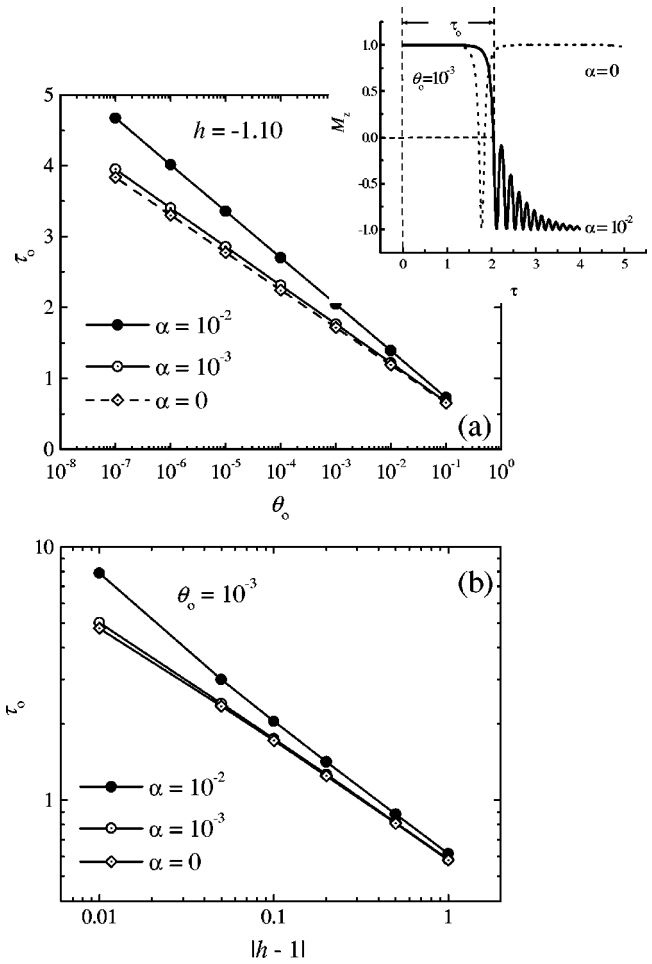

FIG. 10. Initial reversal-related switching time τ_0 for magnetic field-driven reversal. $h_p=190$. Here we define τ_0 as the amount of time it takes for **M** to evolve from θ_0 to $\theta\approx\pi/2$. (a) τ_0 is largely determined by the unperturbed motion of **M**. Adding damping changes the ringing characteristic after the initial reversal, but it does not significantly alter the initial switching time. As shown in the text, an asymptotic relation $\tau\sim-\log\theta_0$ is held for zero (or a small) α. (b) τ_0 scales essentially as $|h-1|^{-1/2}$. Again the result is fairly robust against adding a small α. The top inset shows time dependencies of M_z and the definition of τ_0 in our numerical procedure.

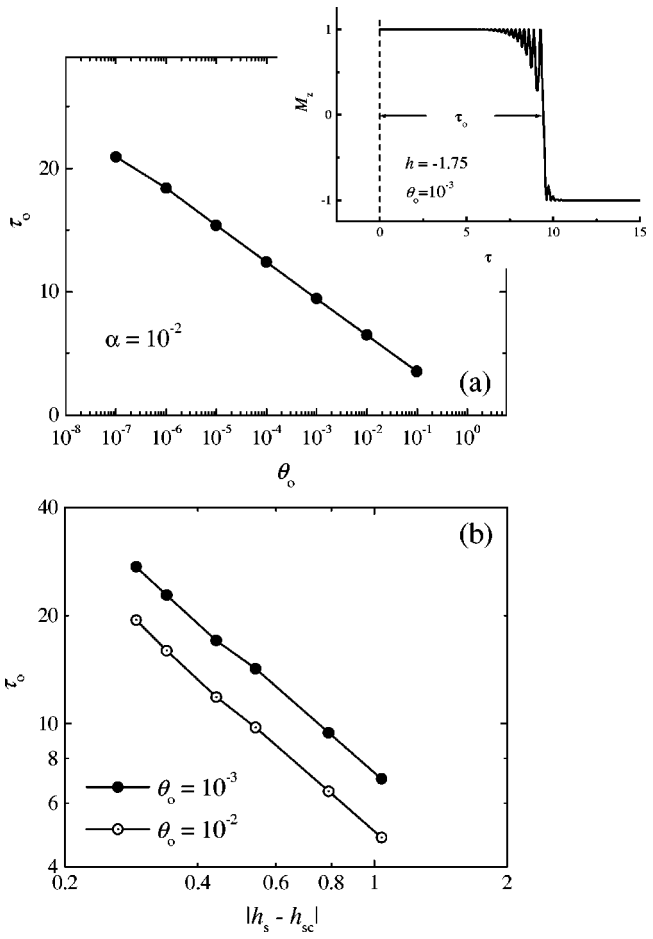

FIG. 11. The reversal process for a spin-current-driven process. (a) Initial reversal-time dependence on starting angle θ_0. A scaling of $\tau_0\propto-\tau_1\ln\theta_0$ is demonstrated, as discussed in the text. (b) The scaling of τ_0 as h_s approaches h_{sc}. It is described by $\tau_0\propto|h_s-h_{sc}|^{-1}$, with h_{sc} as described by Eq. (17). Upper inset shows the time-dependent evolution of $M_z(\tau)$ and the definition of the initial reversal time τ_0.

the $h_p=190$ used in the simulation for Figs. 10 and 11. The time conversion is $t\approx\Omega_k^{-1}\tau=0.568(\text{ns})\tau$ with $\Omega_k=(2\mu_B/\hbar)H_k\approx1.76\times10^9$ s^{-1}. When driven at twice the threshold value, for on-axis-only a magnetic-field-driven switch, and at an initial angle of $\theta_0=10^{-3}$, the initial-reversal part of the switching time is about $t_0\approx0.34$ ns, according to data shown in Fig. 10. With the same amount of overdrive ($h_s=2h_{sc}$), and the same $\theta_0=10^{-3}$, the spin-current driven process will involve a $t_0\approx3.98$ ns.

VI. MATERIALS-RELATED DEVICE CONSIDERATIONS

Equation (18) has important implications for device applications. First of all, there is a fundamental limit on how small the critical current can be if it were to be used for switching a memory element. The limit is set by the memory bit size required for thermal stability. This was briefly discussed in Ref. 7 where the numerical estimates were based on a definition of super-paramagnetic transition temperatures that allows a magnetic lifetime of 1 s. Here we discuss this with a more realistic magnetic stability requirement of 100 yr. The thermal transition lifetime τ_L of the magnetic body can be expressed as $\tau_L=\tau_A\exp(E_0/k_BT)$ with the thermal activation barrier E_0 for moment reversal set by the uniaxial anisotropy barrier height: $E_0=\frac{1}{2}a^2l_mM_sH_k$. τ_A is associated with the basic magnetic attempt frequency with $1/\tau_A\approx10^9$ Hz. If one sets the magnetic lifetime $\tau_L>100$ yr $=3.15\times10^9$ s as criterion for super-paramagnetic transition, this gives a super-paramagnetic transition temperature T_S such that $E_0/k_BT_S\sim\ln(\tau_L/\tau_0)\sim42.60$. Thus $E_0=42.60k_BT_S$ and $a^2l_mM_sH_k=85.19k_BT_S$. From Eq. (18), this means the threshold current for a 100 yr stability against thermal reversal has to be larger than

$$I_c\geqslant\frac{1}{\eta}\left(\frac{2e}{\hbar}\right)\alpha(85.19k_BT_S). \tag{28}$$

Taking $\eta=0.1$ and $\alpha=0.01$ as a conservative estimate of a typical magnetic metal such as cobalt, and setting operating

temperature $T_S = 130\,^{\circ}\mathrm{C} = 400$ K, we have the minimum threshold current for technologically interesting applications of $I_c \sim 140\ \mu$A.

For thin-film devices in current-perpendicular geometry, we can estimate the amount of current density required for magnetic switching. Assume that there are ways to neutralize the demagnetizing field of the film, the threshold current density can then be expressed as

$$J_c = \frac{\alpha}{\eta}\left(\frac{2e}{\hbar}\right)(l_m H_k M_s)\left(1 + \frac{H}{H_k}\right), \tag{29}$$

where l_m can be viewed as the thickness of the magnetic switching layer. The critical current density is then directly proportional to the film thickness l_m. Again, taking cobalt as an example where we assume a uniaxial anisotropy term of $H_k = 100$ Oe, and a saturation magnetization $M_s \simeq 1.5 \times 10^3$ emu/cm^3, in zero-applied field, one has $J_c = 4.6 \times 10^4 l_m (\mathrm{A/cm^2})$, where l_m is in angstroms. An all-metal current-perpendicular pillar can probably take around 10^7 to 10^8 A/cm^2 of current density without short-term damage. This gives a reasonable working film thickness of at least 100 Å. For magnetic tunneling junctions, however, the practical J_c from materials and electrical integrity point of view is limited to about 10^6A/cm^2. This means to directly inject spin current across a tunneling barrier into the magnetic body, the magnetic body would prefer to have softer anisotropy energy product $H_k M_s$ to give a reasonable working film thickness of well-above 10 Å. This can perhaps be done by a careful selection of electrode material and its shape—a low-aspect ratio Permalloy magnetic dot perhaps will work.

Combining the requirements of thermal stability [Eq. (28)] and current-density limit [Eq. (29)], the lateral dimension of the magnetic body can be determined as well. To have a $T_S = 400$ K, again use the parameters for cobalt as we did before, and set $l_m = 15$ Å, one has $a \sim 1500$ Å. These numbers give a rough estimate to the relevant device dimensions, although they should not be taken literally. For one thing at such high aspect ratios it is questionable whether the film will remain single domained for its dynamic processes.

VII. SUMMARY

A preliminary study is presented here for the basic dynamic properties of a magnetic moment under the influence of a spin current. The magnetic moment is found to precess under the torque associated with spin-current-induced angular momentum deposition. The competition between the spin-current-related energy gain and the LLG damping-related energy dissipation determines the precession process. Under appropriate conditions, the precession will lead to a reversal of the resting direction of the magnetic moment, causing a magnetic switch. Quantitative predictions are made for the threshold spin current for such a switch, as well as the general dependence of the switching process on the magnetic environment experienced by the moment. The switching speed under spin-current injection is predicted to be comparable to present-day field-driven switching processes, although the two processes are intrinsically different and they follow different asymptotic scaling behaviors with regard to the initial and drive conditions. The spin current is also predicted to affect the magnetic switching characteristics of the moment, causing a distortion to the astroid-shaped switching characteristics.

ACKNOWLEDGMENTS

I wish to thank John Slonczewski and Roger Koch at IBM Research and Professor Dan Ralph at Cornell University for fruitful discussions. I would also like to thank Roger Koch for help setting up the computing environment for part of this simulation work.

[1] J. C. Slonczewski, J. Magn. Magn. Mater. **159**, L1 (1996).
[2] J. C. Slonczewski, J. Magn. Magn. Mater. **195**, L261 (1999).
[3] L. Berger, Phys. Rev. B **54**, 9353 (1996).
[4] L. Berger, J. Appl. Phys. **49**, 2156 (1978).
[5] Y. B. Bazaliy, B. A. Jones, and S.-C. Zhang, Phys. Rev. B **57**, R3213 (1998).
[6] M. Tsoi, A. G. M. Jansen, J. Bass, W.-C. Chiang, M. Seck, V. Tsoi, and P. Wyder, Phys. Rev. Lett. **80**, 4281 (1998).
[7] J. Z. Sun, J. Magn. Magn. Mater. **202**, 157 (1999).
[8] E. B. Myers, D. C. Ralph, J. A. Katine, R. N. Louie, and R. A. Buhrman, Science **285**, 867 (1999).
[9] J. A. Katine, J. F. Albert, R. A. Buhrman, E. B. Meyers, and D. C. Ralph, Phys. Rev. Lett. **84**, 3149 (2000).
[10] This is a phenomenological assumption that simplifies the math while still keeping the essence of the physics. Details of the spin angular momentum transfer process is significantly more complex, and is certainly interface dependent. Experimental quantification remains to be obtained. A theoretical derivation based on microscopic quantum mechanics for a specific five-layer geometry was given by Slonczewski in Ref. 1, which gave Eq. (6) an additional factor of $(1/\eta)g(\mathbf{n}_s \cdot \mathbf{n}_m) = (1/\eta)[-4 + (1+\eta)^3(3 + \mathbf{n}_s \cdot \mathbf{n}_m)/4\eta^{3/2}]^{-1}$. The angular dependence of this factor is not significant for small η.
[11] J. C. Slonczewski, IBM Research Memorandum No. 003.111.224 (1956). Also see L. D. Landau and E. M. Lifshitz, *Electrodynamics of Continuous Media* (Pergamon, New York, 1960), Sec. 37, pp. 150–151.